CHAPTER 1

General Introduction

1.1 Nanoscience and Nanotechnology

The prefix *nano* in the words nanoscience and nanotechnology derives from Greek word *nanos* meaning *"dwarf"* [1]. It denotes one part of a billion, $1x10^{-9}$ [1-3]. While the prefix *nano* is relatively new, the existence of functional devices and structures of nanometer dimension is long as life itself. Strong shells of an abalone, a mollusk, which contain nanomaterials of calcium carbonate, are a natural example. Knowingly or unknowingly mankind have been encountering the beauty of nanomaterials from earlier time. *Lycurgus Cup*, a 4^{th} century Roman cup which changes color from green to deep red when a light source is placed inside it, is found to contain silver and gold nanoparticles [2,4]. Beautiful colors of window glasses of the medieval cathedrals are due to presence of metal nanoparticles. In 1857, Michael Faraday attempted to explain effect of metal particles on the color of the church windows [2].

Present state of advancement in the field of nanoscience and nanotechnology stem from the classic lecture "*There's Plenty of Room at the Bottom*" given by Richard Feynman in 1959 at Caltech. In his lecture he considered possibility of manipulating materials at atomic scale. He envisions the whole volumes of the *Britannica Encyclopedia* written in a pin head [2,5,6]. Eric Drexler *et al.*, in their well coveted book, *Unbounding the Future*, envision a vast industrial revolution of the unprecedented size and scale [7]. Since then lot of research is carried out throughout the globe on nanoscience and nanotechnology with the purpose of assessing its potentials for technological innovation. As a result new types of materials which possess physical and chemical properties which are not observed in bulk counterpart were discovered [8-11]. In 1985, Harold Kroto and co-workers discovered a new allotrope of carbon, *fullerene* (C_{60}) [9]. In 1990s, Iijima discovered another allotrope of carbon, called *carbon nanotubes*, and phenomena of superconductivity and ferromagnetism were found in C_{60} [2,10]. In 2004, a graphitic films called *graphene* was discovered by Novoselov *et al* [11]. Now, the field garnered increased scientific, political and commercial attention that led to both controversy and progress throughout the World [2,3]. Meanwhile, commercialization of products based on nanotechnology increases day by day. The prefix *nano* is used as a buzzword in books, movies and other commercial items. In future, nanotechnologies hope to provide solutions to all kind of mankind's problems whether it be hunger in the developing countries and pollutions in the developed ones [7].

The Royal Society & The Royal Academy of Engineering, UK define *nanoscience as the study of phenomena and manipulation of materials at atomic, molecular and macromolecular scales, where properties differ significantly from those at a larger scale; and nanotechnologies as the design, characterization, production and application of structures, devices and systems by controlling shape and size at the nanometer scale* [12]. Nanoscience and nanotechnology deal with materials, called nanomaterials, having size scales within 1 to 100 nm, at least in one dimension [2,3]. Literally, 1 nm is the length of ten H-atoms (Bohr radius = 0.5 Å) [3].

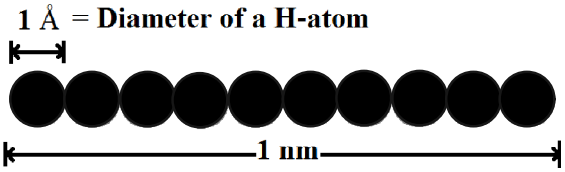

Figure 1.1: Length of 10 hydrogen atoms, which is equal to 1 nm.

The nanomaterial bridges between atoms and molecules to macroscopic and bulk materials (> 100 nm). It exhibits new properties, different from their bulk counterparts, which depend on the material size [2,3,13]. As such, the electronic structure, conductivity, melting temperature, mechanical properties, etc. has been changed when material sizes are lower than a critical size. For example, malleability and ductility of bulk copper are lost when the size is reduced to 50 nm and it becomes super hard material that do not exhibit the same malleability and ductility as bulk copper; gold nanoparticles appear deep red to black in solution as different from ordinary yellowish gold, etc. Size dependent properties allow one to tune the properties of nanomaterials. This is the key to attraction in nanomaterials research. Indeed, surface to volume ratio of nanomaterials increases as the size decreases which makes possible new quantum mechanical effects and hence its properties change as the size changes in nano regime [2,3,8,13].

Among the nanomaterials, crystalline materials called *nanocrystals* are of particular interest. For example, silicon nanocrystals can provide efficient light emission even though bulk Si cannot and can be used for memory components. Nanocrystals can provide single domain crystalline system which can be used to provide information that can help explain the behavior of macroscopic samples of similar materials, without the complicating presence of grain boundaries and other defects [14,15].

Of the different interesting research areas which are encompassed by nanoscience and nanotechnology, research on luminescence properties of nanomaterials is one among them. Production of different colors from the same material by tuning the size of a semiconducting nanomaterial is well established. For example, Cadmium Selenide (CdSe) can be tuned to emit different color by tuning size of the nanomaterial [13,16].

1.2 Photoluminescence

1.2.1 Fluorescence and Phosphorescence

Luminescence is emission of light from a substance by any mechanism other than *black body radiation* or *heat*. This distinguishes luminescence from, *incandescence* which is due to heating. Depending upon the mechanism it follows, there are different types of luminescence. Type of luminescence and its corresponding mechanism are given in **Table 1.1** [17-20].

Table 1.1: Types of luminescence and its corresponding mechanisms.

Types of Luminescence	Mechanism
Chemiluminescence	Chemical reaction
Bioluminescence	Biochemical reaction by a living organism
Electrochemiluminescence	Electrochemical reaction
Crystalloluminescence	Crystallization
Electroluminescence	Electric current passed through a substance
Cathodoluminescence	Struck by electrons
Mechanoluminescence	Mechanical action on a solid
Triboluminescence	Bonds in a material are broken
Fractoluminescence,	Bonds in certain crystals are broken by fractures
Piezoluminescence	Action of pressure on certain solids
Sonoluminescence	Imploding bubbles in a liquid when excited by sound
Photoluminescence	Absorption of photons
Fluorescence	Singlet–singlet electronic relaxation
Phosphorescence	Triplet–singlet electronic relaxation
Radioluminescence	Bombardment by ionizing radiation
Thermoluminescence	Re-emission of absorbed energy when a substance is heated

Characterization by photoluminescence (PL) spectroscopy is the main theme of this thesis and it is discussed in length. *Photoluminescence* is defined as the re-emission of photon from a material when a photon is absorbed by the material [17-20]. Depending upon the re-emission of the photon, it is again differentiated into two

type viz. *fluorescence* and *phosphorescence*. **Figure 1.2** shows a *Jablonski diagram* showing fluorescence and phosphorescence.

In the figure, S_0, S_1, S_2 and T_1 represent ground, first, second singlet excited and triplet states respectively of a luminescent material. Upon absorption of light by the material, it is excited to higher energy states, S_1 or S_2. If excited to S_2, it is rapidly relax to the lowest energy level, S_1. This is called *internal conversion* and occurs within 10^{-12} s or less. Emission from the excited state occurs at a lower energy than absorption due to this internal conversion process [17,21]. The emission can be occurred from S_1 in two different ways. If S_1 jumps to S_0 directly, the type of photoluminescence is called *fluorescence*. On the other hand, if S_1 jumps to S_0 through the triplet state, T_1, then it is called *phosphorescence*. Transition of S_1 to T_1 is called *intersystem crossing*. Transition from T_1 to the singlet ground state is spin forbidden, as a result the transition rate for triplet emission are several times greater than those of fluorescence, i.e., *lifetime* of fluorescence and phosphorescence differ several times. Typical lifetime for fluorescence is 10^{-8} s and that of phosphorescence ranges from millisecond to hours [17-20].

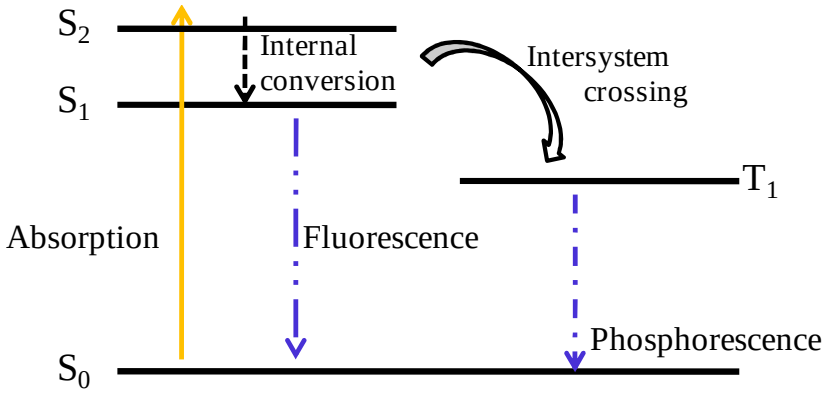

Figure 1.2: Jablonski diagram showing fluorescence and phosphorescence.

1.2.2 Radiative and Non-radiative Transitions

In the luminescence processes described above, not all the energy used in excitation of a luminescent material is emitted as light. Transition from excited state to the ground state can also be without emission of light. Transition which emits light is called *radiative transition* and transition which does not emit light is called *non-radiative transition*. The energy absorbed by the material which is not emitted as light is dissipated to the surrounding in the form of vibrational energy, often referred to as *phonon* emission or more commonly *heat*. Its effectiveness depends on the

availability of high energy vibrations in the surroundings. The fundamental vibrations of chemical bonds in the surroundings are determined by its reduced mass. Especially, bonds with light elements, such as hydrogen, have smaller reduced mass and therefore high vibrational energies. These bonds are therefore able to take up large amount of energy and effectively contribute to non-radiative transition. It is therefore imperative to suppress such bonds and hence the non-radiative transition; since one of the most important requirements of luminescent is high light output, which is radiative [16,17,21]. The two transitions always compete with each other and give rises to lifetime, quantum yield, quenching, etc. discussed below.

1.2.3 Lifetime

Lifetime *(τ)* is one of the most important characteristics of a luminescent material. It determines time available for the material to interact with exciting photons or diffuse the photons in its environment. When a sample is excited with a sharp pulse of light, an initial population (n_0) of the sample is in excited state. For a two level system i.e., ground state and exited state, the population of the excitation state decays with a rate $\Gamma + k_{nr}$ according to

$$dn(t) / dt = - (\Gamma + k_{nr})\, n(t) \qquad (1.1)$$

where $n(t)$ is the number of excited molecules at time t following the excitation pulse; Γ is radiative decay and k_{nr} is non-radiative decay to the ground state [17,21]. Emission is a random process and each excited molecule/ion has the same probability of emission in a given interval of time. This results in an exponential decay of the excited state population,

$$n(t) = n_0 \exp(-t/\tau) \qquad (1.2)$$

where $\tau = 1/(\Gamma + k_{nr})$ is the lifetime of the sample. The number of excited molecule/ion, $n(t)$, is not observed in photoluminescence experiment, but photoluminescence intensity, $I(t)$, is observed. The two are related as $I(t) \propto - dn(t)/dt$. Therefore, the above equation can be written in terms of time dependent intensity, $I(t)$ as:

$$I(t) = I_0 \exp(-t/\tau) \qquad (1.3)$$

where I_0 is the intensity at time 0 (zero). Hence, the photoluminescence lifetime can be determined from the plot of log $I(t)$ vs. t, but more commonly by fitting the decay data to assumed decay models [17,21].

The emission of light is a random process and few molecules/ions emit photons at precisely $t = \tau$. After a time τ the population of the excited state has

decreased to *1/e* (37%) and the rest (63%) have decayed prior to $t = \tau$. Therefore, the lifetime of the excited state can also be defined as average time the molecules/ions spend in the excited state prior return to the ground state [17,21]. This can be observed by calculating the average time in the excited state as:

$$<t> = \int_0^\infty tI(t)dt / \int_0^\infty I(t)dt \quad (1.4)$$

or, $$<t> = \int_0^\infty t\, exp(-t/\tau)dt / \int_0^\infty exp(-t/\tau)dt = \tau. \quad (1.5)$$

[Since, *Gamma function*: $\int_0^\infty x^m\, exp(-ax)dx = \Gamma(m+1)/\, a^{m+1}$; *m* is positive]

It is to be noted that the above equation (1.5) is not true for more complex decay laws, such as multi- or non-exponential decay laws. However, by using an assumed decay law, the average lifetime can always be calculated from the equation (1.4). For example, the average lifetime $<t>$ for bi-exponential decay is:

$$<t> = (I_1\tau_1^2 + I_2\tau_2^2) / (I_1\tau_1 + I_2\tau_2) \quad (1.6)$$

where $I = I_1\, exp\{-(t/\tau_1)\} + I_2\, exp\{-(t/\tau_2)\}$, is the bi-exponential decay law; I_1 and I_2 are intensities at two different values of time *(t)*, τ_1 and τ_2 [19,21,22].

1.2.4 Quantum Yield

Quantum yield (QY), denoted by η, is also one of the most important characteristics of a photoluminescent material. It is defined as the number of emitted photon relative to the number of absorbed photons [16,17,19,21,23,24]. Considering the sample in the excited state, the excited state depopulate to the ground state through radiative (Γ) and non-radiative (k_{nr}) decays. The fraction of radiative emission to the ground state is the quantum yield i.e.

$$\eta = \Gamma / (\Gamma + k_{nr}). \quad (1.7)$$

Sample with the largest quantum yield displays the brightest emission. It is a factor which determines the efficiency of a luminescent material. It can be close to unity if the radiative rate of transition is much greater than that of non-radiative transition. However, it is always less than unity because of *Stokes shift* [21].

1.2.5 Quenching

Not only lifetime and quantum yield depend on the non-radiative rate, but luminescence intensity also depend on the non-radiative rate of transition. Because of non-radiative transition, the intensity of luminescence decreases. Such decrease in the intensity is called *luminescence quenching* [16,17,19,21]. Oxygen molecule, O-H group, halide elements, etc. are well known quenchers. Luminescence quenching can

also be occurred due to various mechanisms, such as multi-phonon emission, cross relaxation, up-conversion, energy transfer between same luminescent centers, energy transfer between different luminescent centers, etc [16,17,21,25]. Energy transfers between luminescent centers are unavoidable to a doped nanocrystal. For a doped nanocrystal, large concentration of the dopant and small crystal size plays a great role in quenching [16,26,27]. In chapter 5, quenching due to large concentration or concentration quenching and quenching due to small crystal size or size quenching of the synthesized ZrO_2:Eu^{3+} nanocrystals are reported exhaustively.

1.3 Photoluminescence of Europium Ion (Eu^{3+})

Luminescence of lanthanide ions has found applications in medical diagnostics, laser, optical fiber, night vision goggles, sunglass lenses, cathode ray tube (CRT), etc. Early CRT of color television had poor quality red color. Europium as a phosphor dopant made the quality of the red color good [16,17,25]. Recently, with the advancement of nanoscience and nanotechnology lanthanide luminescence has been using in treatment of diseases. It is used in *drug delivery* and *nanomedicine* as a tracker of drugs delivered to specific diseased cells [28-30].

Europium is a lanthanide element and lanthanide ions are characterized by spectral peaks whose positions are independent of host matrix [16,18,25]. The Eu^{3+} peaks results from transitions within *4f* shell which are shielded from surrounding by filled *5s*, *5p* and *6s* shells, which are lower in energy, but spatially located outside the *4f* orbital. Interactions leading to different electronic energy levels for the *[Xe] $4f^6$ $5d^0$* configuration of Eu^{3+} and hence the different peaks are shown in **Figure 1.3**. Coulombic interaction which represents the electron-electron repulsions within the *4f* orbital is the largest interaction among the *4f* electronic interactions. This interaction yield terms with a separation of the order of 10^4 cm^{-1}. These terms are split into several *J*-levels according to spin-orbit coupling with a separation of the order of 10^3 cm^{-1}. The individual *J*-levels are further split when the ion is presented in a coordinating environment such as a crystal which is referred to as crystal field splitting. The crystal field splitting is of the order of 10^2 cm^{-1} and it gathered information about the symmetry of the coordinating environment [17,18,25].

The main emissions of Eu^{3+} occur from $^5D_0$ to ^7F_J (J = 0, 1, 2, 3, 4, 5, 6) levels. The $^5D_0 \rightarrow {}^7F_1$ transition is a pure *magnetic dipole transition*. This transition is practically independent of host matrix. The transitions from $^5D_0$ to the ^7F_J (J = 2, 4, 6)

are pure *electric dipole transition* and they are strongly sensitive to symmetry of the host matrix. The remaining transition to ^7F_J (J = 0, 3, 5) levels are forbidden both in magnetic and electric dipole transitions and are usually found to be very weak in emission spectrum [16-18,25].

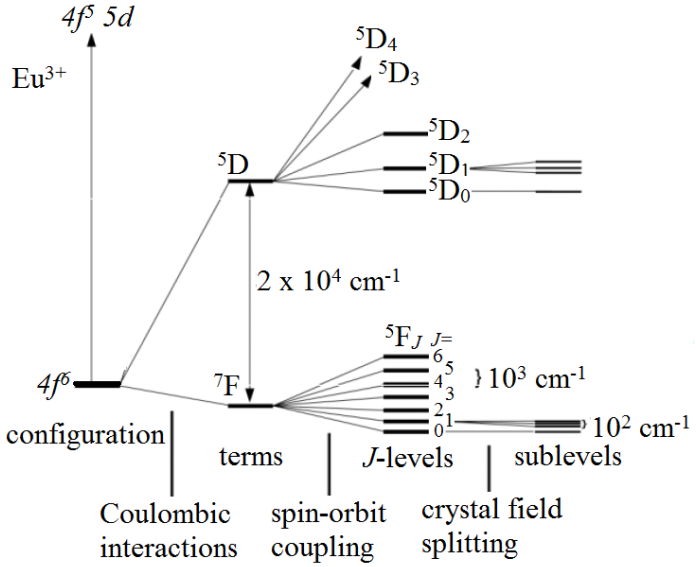

Figure 1.3: Electronic energy levels for the $[Xe]^4f^6\ 5d^0$ configuration of Eu^{3+}.

When introduce in a host material, lanthanide ions effectively deactivated non-radiatively in organic host. On the other hand, inorganic hosts such as glasses and crystals have less effective non-radiative deactivation channels for excited lanthanide ions. However, absorption band of lanthanide ions are weak in inorganic hosts. A means to obtain efficient light absorption is the incorporation of lanthanide ions to semiconducting nanocrystals [16,25]. Therefore, selections of inorganic hosts which are semiconducting and nanocrystalline in nature may best suit the photoluminescence study of lanthanide ions doped materials.

1.4 Zirconia or Zirconium Dioxide (ZrO_2)

Zirconia or zirconium dioxide (ZrO_2) is an inorganic semiconductor. It is an attractive material in both fundamental and application-oriented research. Because of its high melting point, high thermal and mechanical resistance, high thermal expansion coefficient, low thermal conductivity, high thermochemical resistance, high corrosion resistance, high dielectric constant and photothermal stability, it has extensive applications in photonics and other industries [31-34]. It is used as refractory, artificial teeth, diamond simulant, among others [35-39]. As a refractory material, it is used in installations for growing single crystals [40]. In dentistry, it is

used for dental reconstruction [39,41]. Its color or brilliance does not lose as diamond and variety of colors are available. It occupies the largest gemstone in jewelry market [42]. High chemical and photochemical stability with high refractive index and low phonon energy makes it an ideal medium for preparation of highly luminescent materials [31-34,43].

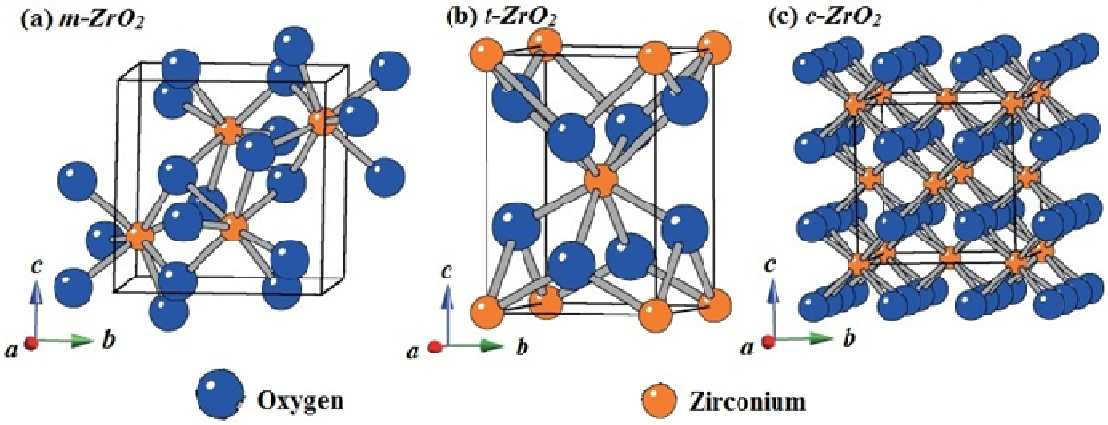

Figure 1.4: Crystal structures of (a) monoclinic, *m-ZrO_2*; (b) tetragonal, *t-ZrO_2* and (c) cubic, *c-ZrO_2*.

Zirconia has generally three crystal structures viz. *monoclinic* (<1170 °C), *tetragonal* (1170 °C-2370 °C) and *cubic* (>2370 and 2706 °C) [31,32,36]. **Figure 1.4** shows the three crystal structures of ZrO_2. Its crystal structures significantly influences its properties [35]. Fortunately, the crystalline structures of zirconia can be tailored in many ways. Among them annealing of precursor and/or introducing a dopant to the host zirconia are observed to be easiest [36,44-47]. Alarcon reported that increasing annealing temperature to the zirconia obtained from gels transform its structure from tetragonal to monoclinic. Further, formation of monoclinic zirconia took place on doping vanadium on the gel [46]. On the other hand, Srdić *et al.* reported that introduction of aluminum on the zirconia host can decrease fraction of monoclinic phase and stabilized to tetragonal or cubic phase [47]. On the same line as that of Srdić *et al.*, Chen *et al.* reports on the transformation of monoclinic to tetragonal phase on doping europium in zirconia [44]. Interestingly, on close observation of the reports, it is found that the change in the phases of zirconia is a result of oxygen vacancy. That is, oxygen evolution results in transformation to more stable phase, while oxygen reduction results to less stable phase of zirconia [36,44,45,48]. Because of the oxygen vacancy, zirconia has a broad emission in violet or blue region of visible spectrum [36,44,49]. This emission may be altered for a specific requirement by introducing a dopant to the host zirconia. For example, when

red emitter, Eu^{3+}, is introduced in the host zirconia the resulting color of emitted light may no longer be violet or blue. Depending upon the type and concentration of dopant the color of emitted light may be tuned [19,50,51]. Apart from tuning the color, introduction of dopant on the zirconia host can tune size of zirconia crystal in accordance with *Bragg's law* and *Scherrer formula* of x-ray diffraction [52-54]. For example, if a bigger ionic size such as Eu^{3+} (98 pm) replaces Zr^{4+} (87 pm) of ZrO_2, the crystal size can be reduced on increasing the doping concentration. This is illustrated in chapters 3 and 5. In view of these facts, synthesis of doped nanocrystals attracted researchers for manipulation of crystal sizes and hence the properties.

1.5 Synthesis of Nanocrystals

Beauty of nanoscience and nanotechnology lies in the fact that properties of the nanomaterial can be engineered as a function of its size. That is, production of a particular property needs synthesis of proper material size. However, synthesis of the required material size required proper synthetic techniques. Broadly there are two approaches for fabricating nanomaterials. One is *bottom-up* and the other is *top-down*. As the name indicates, in top-down approach, large or bulk materials are chopping down to get a smaller material sizes of required dimension. LASER itching, molecular beam epitaxy, photolithography, ball mining, etc., are some examples for fabrication of nanomaterials by top-down approach. Top-down approach is not economical and hence it is not preferred for synthesis of nanomaterials. On the other hand, bottom-up approach gives a means to synthesize nanomaterials economically. In bottom-up approach, atoms and molecules are aggregate to form nanomaterials of required dimensions. Examples of bottom-up approach are vacuum evaporation, sputtering, combustion, pulse LASER deposition, solvothermal, precipitation, etc. The bottom-up approach is easily achieved by *wet chemical method*. Precipitation is one of the most easy and economical wet chemical method for synthesis of nanomaterials [16,19,25,50]. In this approach, required compositions of the nanomaterial to be synthesized are mixed in a specific solvent. Then a precipitating agent is added to the solution. The precipitate so obtained is a precursor for the required nanomaterial. Usually, the size of the nanomaterial can be tuned by adding a *capping agent*. It is an agent which restricts or caps the growth of nanomaterials during reaction. The size of crystalline nanomaterial can also be tuned by annealing the precursor at high temperature. In solvothermal (such as hydrothermal), nanomaterials grow in a

solution of precursor materials at elevated pressure and temperature. Pressure and temperature are the parameters that can be controlled to tune the material size [16,25,55].

Currently, lanthanide doped nanocrystals are active area of research especially using wet chemical methods [16,19,20,25,50,56]. The present thesis employed wet chemical precipitation techniques viz. polyol, hydrothermal and simple precipitation for synthesis of ZrO_2 and ZrO_2:Eu^{3+} nanocrystals. Details of the synthesis techniques will be found in the following chapters.

1.6 Instrumentation and Characterization

Instrumentation and characterization are the most important parts in nanomaterial research. It is only through the instrumentations which make possible to characterize and discover the unique properties of nanomaterials. Indeed nanoscience and nanotechnology gained popularity for the properties of nanomaterial depends on material size and shape. Nevertheless, one cannot estimate the size and shape of a nanomaterial without the use of microscopy techniques viz. TEM, SEM, AFM, etc [19,20]. Crystallinity of nanomaterials can be checked by XRD, TEM, HRTEM and SAED, etc. In view of these facts, instruments used for characterizations of the synthesized ZrO_2 and ZrO_2:Eu^{3+} nanocrystals viz. powder XRD, TEM, HRTEM, SAED, FT-IR, EDAX on SEM, PL, etc. are elucidated as under:

1.6.1 Powder XRD

X-ray diffraction (XRD) is a versatile, non-destructive characterization method used for determining atomic and molecular structure of a crystal; crystal size, stress measurement, etc [19,57]. It works on the principle of *diffraction*. A crystal is a periodic arrangement of atoms or molecules and hence it can act as scattering centers for x-rays. Electrons around the atoms or molecules are responsible for elastic scattering of the x-rays resulting the diffraction. If x-ray falls on these periodic arrangements of atoms or molecules, destructive and constructive diffraction occurred according to *Bragg's law*:

$$2d_{hkl} \sin\theta = \lambda \qquad (1.8)$$

where d_{hkl} is the interplanar spacing; θ is the incident angle (*Bragg angle*) and λ is the wavelength of the incident x-ray used [19,20,50,56,57]. **Figure 1.5** shows the schematic diagram of x-ray diffraction by a crystal for derivation of *Bragg's law*.

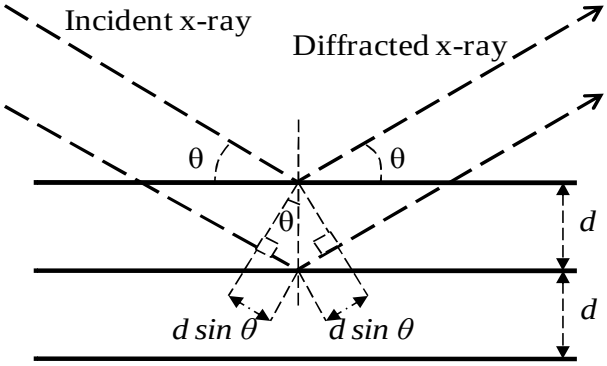

Figure 1.5: Schematic diagram of x-ray diffraction and Bragg's law.

Basic components of a powder x-ray *diffractometer* consist of an x-ray source, a sample stage and a detector. The x-ray is focused on the sample at an angle θ, while the detector opposite the source reads the intensity of the x-ray it receives at 2θ away from the source path. The incident angle is than increased over time while the detector angle always remains 2θ [19,20,50,56,57]. **Figure 1.6** shows a schematic diagram of the basic components of x-ray diffractometer.

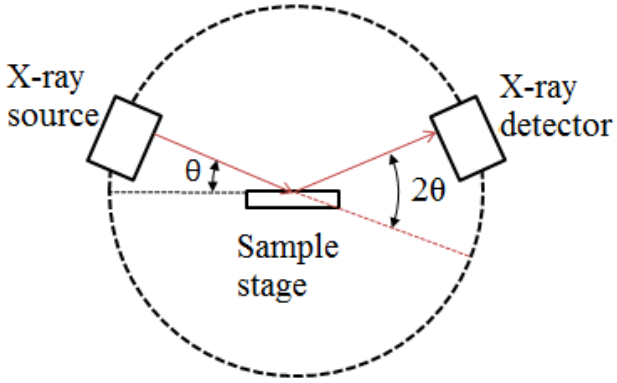

Figure 1.6: Schematic diagram of x-ray diffraction showing basic components.

For a typical powder XRD measurement, powder or *polycrystalline* sample to be studied is placed on the sample stage. By assigning a required voltage and current, 40 kV and 30 mA (say), data are recorded within a desired range of angle *(2θ)*, 10 to 90° (say). Since the powder sample contained a large number of crystalline planes oriented in different direction, so called polycrystalline, different peaks are observed in an intensity (or counts) vs. angle *(2θ)* pattern. The observed pattern of sample in study is then compared with JCPDS (Joint Committee on Powder Diffraction Standards) or ICDD (International Centre for Diffraction Data) database of XRD patterns. The reference code consistent with the observed pattern of the sample is noted. Hence, the crystalline samples are characterized by XRD.

The observed peaks of XRD patterns can be used for calculation of crystal size *(t')* of the samples by using *Scherrer formula*:

$$t' = (0.9\,\lambda)/(B\cos\theta) \quad (1.9)$$

where *0.9* is a constant assuming the crystal to be spherical; λ, the wavelength of the x-ray used; *B*, full width at half the maximum intensity (FWHM) in radian and θ, *Bragg angle* [19,20,50,53,54,56]. The FWHM is generally large for a small crystal as in the case of nanocrystals and small for bulk crystal. Besides the crystal size, lattice parameters of unit cell (i.e., *a, b, c* and α, β, γ) can also be calculated from the XRD data.

1.6.2 TEM, HRTEM and SAED

Transmission electron microscopy (TEM) is a major analysis method in a range of scientific fields. It is especially important in nanoscience and nanotechnology where material sizes matter. It is a microscopy technique whereby a beam of electron is transmitted through an ultra-thin specimen and image so formed is observed in a detector. Its working is based on the wave nature of electrons. The wavelength *(λ')* of electron is related to their kinetic energy *(E)* via *de Broglie equation*:

$$\lambda' = h/(2m_0E)^{1/2} \quad (1.10)$$

where *h* is the Planck's constant and m_0 is the rest mass of the electron.

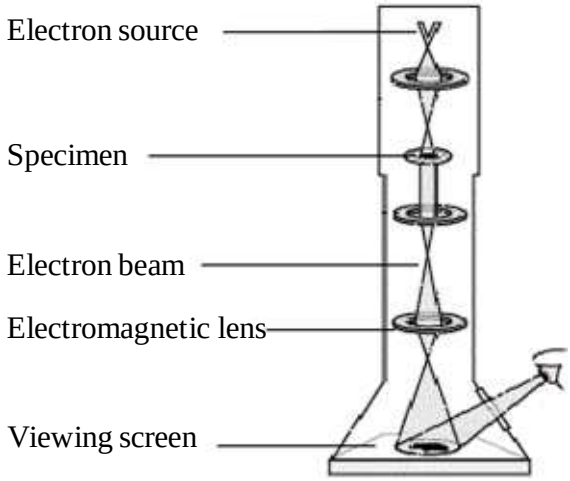

Figure 1.7: Schematic diagram of a TEM.

Figure 1.7 shows the schematic diagram of a TEM. Its basic components include a vacuum system through which a beam of electrons travels, source of the electron beam, specimen stage, electromagnetic lenses and detectors. To increase mean free path of electro-gas interaction the system is evacuated to low pressure, 10^{-4}

Pa (say) and high voltage, 160 kV (say), is applied to generate high energy electron beam [19,20]. At such high energy, the velocity of the electron approaches *c*, the speed of light. Therefore, a relativistic correction is needed to the wavelength of the electron given in equation (1.10) as:

$$\lambda' = h /[2m_0E\{1+(E/2m_0c^2)\}]^{1/2}. \quad (1.11)$$

Theoretically, resolution, *d* (i.e., the capability of an optical system to distinguish, find, or record details) of a microscope is directly proportional to wavelength, λ' as:

$$d = \lambda' /2NA \quad (1.12)$$

where *NA* is the numerical aperture of the system. Since de Broglie wavelength of electron (= 2.85×10^{-3} nm at 160 kV) is about one million times shorter than the wavelength of visible light (400-700 nm), TEM can magnify about one million times than optical microscope. At higher voltage, the de Broglie wavelength of electron can be made still lower and hence higher the resolution of the TEM. High resolution TEM (HRTEM) can directly observed the atomic arrangement of a sample. At present the highest point of resolution is 0.047 nm [58]. At this length scale individual atom of a crystal and its defects can be resolved [58-60].

Like x-ray diffraction, electron beam can also be diffracted through the crystal lattice inside a TEM. Selected area electron diffraction (SAED) gives a set of diffraction spots or rings of a crystal lattice when a high energetic beam of electron is diffracted from the lattice. Spots are obtained for single crystals and rings are obtained for polycrystalline materials. The rings are faded for nanocrystals since limited number of lattice plane are present in the nanocrystals [61]. Particular area of a crystal can be selected to obtain SAED and hence the name '*selected area*'. The diffraction rings of SAED can be used for determination of *interplanar spacing*, d_{hkl} of a crystal. The interplanar spacing can be calculated from *camera equation* given below:

$$d_{hkl} = (L\lambda') / R \quad (1.13)$$

where *L* is the camera length, a constant for the particular TEM; λ', wavelength of electron and *R* is the radius of a diffraction ring. The d_{hkl} calculated from the camera equation can be effectively used for identification of crystal structure. Relative to XRD, it is a more convenient tool for characterization of a crystalline material of small quantity. Because it can examine sample area in nanometer range, while XRD needs several millimeters of sample area to examine.

For a typical sample preparation of TEM, HRTEM or SAED analysis, the sample is ground to powder and disperses in a dispersible liquid. Then a drop of dispersed sample is put on a carbon coated copper grid. Then it is inserted into the instrument with a sample holder. Then the system is evacuated to low pressure ~$1x10^{-4}$ Pa. After that the sample is scanned for TEM, HRTEM images or SAED rings by applying high voltage.

1.6.3 EDAX on SEM

Energy dispersive analysis of x-ray (EDAX) is a characterization technique used for elemental analysis of a sample. It relies on the fact that each element has a unique atomic structure allowing unique set of peaks on its x-ray spectrum, also called *characteristic x-ray* [62]. According to *Moseley's law*, energy (*E'*) of characteristic x-rays emitted from a chemical element is directly proportional to the square of its atomic number, *Z* as:

$$E' = C_1 (Z-C_2)^2 \qquad (1.14)$$

where C_1 and C_2 are constants. If the energy of a given K, L or M line is measured, then the atomic number of the element producing that line can be determined [62]. **Figure 1.8** shows a schematic diagram of electronic transitions giving rise to K, L and M lines.

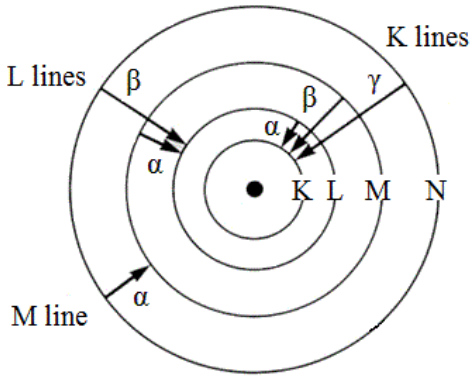

Figure 1.8: Schematic diagram of electronic transitions in an atom.

The EDAX system has six basic components: (1) sample stage and sample chamber on which the sample to be examined is kept; (2) a vacuum system which evacuate air inside the sample chamber; (3) a source of high energy radiation (such as electron beam) which initiate the emission of characteristic x-rays from the sample; (4) an x-ray detector which detect x-rays and convert into electronic signals; (5) a pulse processor which measures the electronic signals to determine the energy of the

x-ray detected; and (6) a multi channel analyzer which displays and interprets the x-ray data [62,63].

For a typical elemental analysis of a sample by EDAX, the powder sample is fixed on a carbon coated tape. Then it is introduced inside the sample chamber of a SEM (Scanning Electron Microscope). After that the chamber is evacuated to low pressure ~ $1x10^{-4}$ Pa. Subsequently, the sample is zoomed to scale of 5 μm (say) and scanned by applying high voltage, 20 kV (say). Then, EDAX data from three different areas of the sample are recorded and average of which is taken as elemental compositions of the sample.

1.6.4 FT-IR

An infrared spectrum represents a fingerprint of a sample with absorption peaks which correspond to the frequencies of vibrational bonds of the atoms which constitute the sample. Since no two compounds have same atomic combination, no two compounds produced the same infrared spectrum and hence infrared spectroscopy can effectively be used for identification of different samples [64-66].

The original infrared spectroscopy is of dispersive nature where prism or grating is used as a dispersive medium of frequencies emitted from an infrared source. And a detector measures the amount of energy at each frequency which has passed through the sample. This results in slow scanning process over the entire frequency range. However, all of the frequencies can be measured simultaneously rather than individually by using an *interferometer*. The interferometer generate a signal called *interferogram*, which has the unique property that every data point which makes up the signal has information about every infrared frequency which comes from the source. This means that all the frequencies are measured simultaneously as the interferogram is measured. And this results in extremely fast measurement. However, the measured interferogram cannot be interpreted directly and hence a means of decoding the individual frequencies is required. This is accomplished by a means of a mathematical technique called *Fourier transform* and hence the name Fourier Transform Infrared (or FT-IR) spectroscopy [64-66].

To measure a typical FT-IR spectrum of a sample, at first, a background or reference (without the sample) is measured. That is, a thin ~1 mm translucent pellet of KBr is scanned. Measurement of KBr pellet makes possible identification of impurities in the KBr and instrumental artifacts, which may alter the real identity of

the sample, if present. Then spectrum of the sample is measured by making a pellet, which is a mixture of the sample and KBr in the ratio ~ 1:100.

1.7 Photoluminescence Spectroscopy

1.7.1 Excitation and Emission Scans

An emission spectrum is the intensity vs. wavelength distribution of an emission measured at a single constant excitation wavelength, generally excitation maximum. Conversely, an excitation spectrum is the intensity vs. wavelength distribution of an excitation measured at a single constant emission wavelength, generally emission maximum. Such spectra can also be presented on *wavenumber* scale. However, wavelength scale is easier to interpret visually. To obtain accurate corrected spectra are difficult and therefore directly recorded uncorrected spectra are generally used [21, 22, 67].

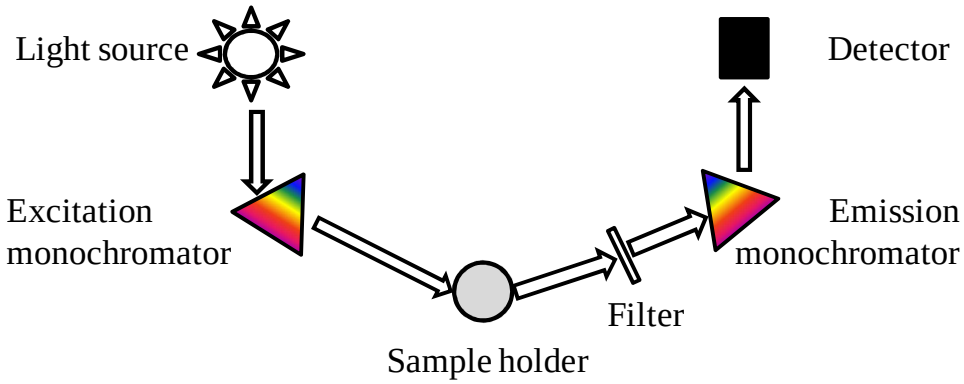

Figure 1.9: Schematic diagram showing general layout of a PL spectroscope.

Recording an excitation or emission spectrum is not an easy task and it differs slightly from one instrument to another. It needs thorough knowledge of the sample under study and thorough knowledge of parameters used in recording the spectra such as slit width, optical filters, etc. **Figure 1.9** shows the basic components of a PL instrument. The basic components include a light source; excitation and emission monochromators; sample holder; optical filters and detector. The light source is a source of white light, like continuous-xenon lamp, which can provide an optimal light output from below 250 to more than 1000 nm. Monochromators are then used to disperse white or polychromatic light into various colors or wavelengths. This makes possible to select a single excitation or emission wavelength to perform an emission or excitation scan [21,22,67]. To perform an excitation scan, the emission monochromator is set at the desired single wavelength and then the excitation

monochromator is scanned through the required wavelength range. The excitation scan range is typically at shorter wavelength than the fixed emission wavelength. On the other hand, emission scan is performed by choosing an appropriate excitation wavelength and emission monochromator is scanned through the required wavelength range. The emission scan range is typically at a longer wavelength than the fixed excitation. Light intensities from the excitation and emission monochromators are controlled by excitation and emission slit widths. To obtain better resolution and signal-to-noise ratio of spectra, large emission slit width and small excitation slit width are assigned for excitation scan, while large excitation slit width and small emission slit width are assigned for emission scan [21,22,67]. In addition to monochromators, *optical filters*, which transmit light above the stated wavelength and block off light below, are often needed to remove unwanted wavelengths in the excitation beam or to remove scattered light from the emission spectrum. A detector detects the light emitted from the sample as photon flux. This is usually performed by a PMT (photomultiplier tube). A PMT is a current source where the current is proportional to the light intensity or number of photons. A PMT multiplied the individual photons and detected as an average signal or counted as individual photons [21,22,67].

For a typical excitation scan, a desired emission wavelength 613 nm (say) is monitored and the excitation monochromator is scanned throughout the required excitation wavelength range, 200 to 400 nm (say). In doing so, an optical filter of 515 nm (say), which is within the maximum value to be scanned (400 nm in this case) and the monitored emission wavelength (613 nm) is selected. The filter remove second order artifact, in this case 306.5 nm (half of 613 nm), which might have creep and alter the excitation spectrum, if the filter has not been used.

Similarly, an excitation wavelength, 286 nm (say), is monitored in recording an emission spectrum, 400 to 700 nm (say). In this case, a filter of 350 nm (say), which is between the monitored excitation wavelength (286 nm) and minimum value of emission (400 nm) is selected. This filter remove second order artifact at around 572 nm (double of 286 nm) which might have creep and alter the emission spectrum, if the filter has not been used.

It is always useful to know sample's absorption or emission before making emission or excitation scans. Even if proper spectroscopy data are not available, looking at the sample can provide valuable information. For example, samples that are

transparent will most likely absorb in the UV and are likely to emit (if indeed there is emission) in the blue region of electromagnetic spectrum. Samples that have yellow color will absorb in the 400 nm region and will probably emit green or orange; samples that are blue will absorb at around 600-700 nm and will have dark red or even infrared emission [22]. However, if both the excitation and emission wavelengths of the sample are unknown then pre-scans are required to know either excitation or emission wavelength. In such case, a random value of excitation wavelength may be monitored and scanned throughout the entire range of emission wavelength. The maximum intensity of the emission spectrum is selected and corresponding excitation spectrum is then recorded. The excitation maximum may not be the wavelength selected in recording the emission spectrum but it is the required excitation wavelength to be monitored in recording an emission spectrum of the sample to give maximum emission intensity. Further, validity or correctness of the sample's emission spectrum can be checked by comparing the color of light observed by naked eyes and the color of light determined from CIE (*International Commission on Illumination*; from French, *Commission Internationale de l'éclairage*) chromaticity co-ordinates and CIE diagram [68,69].

1.7.2 Lifetime Measurement

The basic instrumentation for measurement of photoluminescence lifetime is same as that of excitation and emission scans. According to requirement, the exciting light source may be changed to microsecond flashlamp, nanosecond flashlamp or picoseconds pulsed diode lasers [21,22,67]. Recording of decay curve for measurement of photoluminescence lifetime requires background knowledge of sample to be measured, i.e. knowledge about the absorption and emission properties. Therefore, excitation and emission scans are desirable before attempting lifetime measurement. Usually, the wavelengths corresponding to excitation maximum and emission maximum are selected for measurement of lifetime. After the measurement of decay curves, the measurement is typically analyzed by fitting to a model function of one or more exponential parameters [22]. This will be elucidated in chapters 2, 4 and 5.

1.7.3 Quantum Yield Measurement

Accurate and reliable measurement of quantum yield is tedious and quite time

consuming. It can be measured using a relative method by comparing luminescence parameters to a quantum yield standard; or it can be measured by absolute method. In this thesis quantum yield is measured by absolute method. In absolute method, number of absorbed photons of a sample and the number of consequently emitted photons are directly measured. This is done by using an Integrating Sphere (IS). The IS consists of a 120 mm inside diameter spherical cavity, which is machined from BENFLEC block. This is then surrounded by an aluminum shell for handling and protection. The IS has two perpendicular ports (holes), one with a lens to focus the excitation beam into the sample (kept inside) and a window to collect a portion of the light scattered off the sphere's inner surface [23,24]. The IS has a rotating fold mirror which can be accessible from outside the IS by a knob. The knob can be fixed at "CUVETTE" or "POWDER" according to direct or indirect measurements taken as a part of QY measurement. For a solid sample, the knob at the "POWDER" position indicates direct measurement while the the knob at the "CUVETTE" position indicates indirect measurement. Similarly, for liquid sample, the knob at the "POWDER" position indicates indirect measurement while the knob at the "CUVETTE" position indicates direct measurement. Direct measurement allows the light towards the sample location and indirect measurement allows the light to the sphere's inner surface. The indirect measurement enables subtraction of indirect illumination of the sample by re-excitation of light reflected from the sphere. This re-excitation causes an error in true QY and can be removed by indirect measurement. Thus, the QY (η_1), which is defined as the percentage of photons emitted (ε) by a sample when a given number of photons are absorbed by the sample (α), i.e.

$$\eta_1 = \varepsilon/\alpha = \int L_{direct} / (\int E_{without} - \int E_{direct}) \quad (1.15)$$

can be considered more accurately by using the following equation which take into account the indirect measurement:

$$\eta_2 = (E_{indirect} L_{direct} - E_{direct} L_{indirect}) / (E_{indirect} E_{without} - E_{direct} E_{without}) \quad (1.16)$$

where L_{direct} is the emission spectrum of the sample; E_{direct} is the emission spectrum of the exciting light recorded with the sample in place; $E_{without}$ is the emission spectrum of the exciting light with only the reference in the sphere; $E_{indirect}$ is the emission spectrum of the excitation light recorded with the sample in place but the mirror set to cuvette (for solid sample) and $L_{indirect}$ is the emission spectrum of the sample with the sample in place but the mirror set to cuvette (for a solid sample) [23,24,70].

Experimentally, the parameters of the equation (1.16) can be obtained by scanning only three emission scans. The first scan is the direct emission scan of the reference with the knob of the mirror positioned in "POWDER" (for powder sample). The second scan is the direct emission scan of the sample with the knob of the mirror positioned in "POWDER" (for powder sample). And the third scan, indirect emission scan of the sample with the knob of the mirror positioned in "CUVETTE" (for powder sample). The scan parameters such as slit width, excitation wavelength, etc. are kept unchanged during the three emission scans. The ranges of the emission scans are selected so as to include the excitation wavelength i.e. it starts from a wavelength ~20 nm before the excitation wavelength. Then the three emission spectra are corrected using correction files of the IS. The corrected spectra are used in the equation (1.16) with the help of a wizard called *"Quantum Yield Calculation"* for accurate measurement of QYs [24].

1.8 CIE Chromaticity

Color of light emitted from a sample can be visualized well, if the emission spectrum is simple. For example, if the sample has only a sharp emission peak at 540 nm, it can be known from the knowledge of visible spectrum that the color of light emitted is green. However, if the sample has multiple emission peaks in the emission spectrum, the color of light emitted by the sample cannot be visualized easily. For example, white light sources such as xenon lamp, RGB LED, etc. have multiple emission peaks within the visible range. In such case, CIE chromaticity diagram and

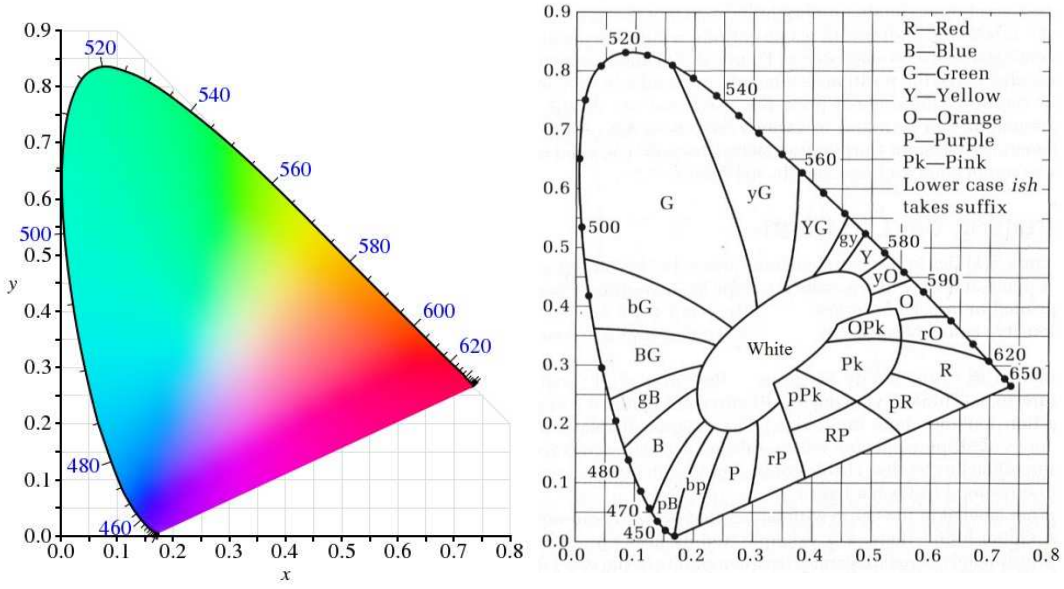

Figure 1.10: (a) The CIE 1931 color space chromaticity diagram and, (b) black and white representation of (a).

co-ordinate can be effectively used to determine the color of light emitted by the sample. Further, it is important in phosphor research where UV light is usually used to excite the phosphor for generation of light. If naked eyes are used to observe the color of light emitted from the phosphor, instead of the CIE chromaticity diagram and co-ordinate, the eyes may get damaged due to the dangerous UV light.

The CIE chromaticity diagram is horseshoe-shaped with its curved edge corresponding to all spectral colors with wavelength shown in nanometer, and the remaining straight edge corresponding to the most saturated purples, mixtures of red and violet, **Figure 1.10(a)** [19,68,69]. Depending on the calibration of display devices or type of printers, used to see the diagram, the chromaticity diagram may not be displayed properly. Therefore, black and white representation of the diagram is shown in **Figure 1.10(b)**, where the colors are leveled [68,69].

The CIE XYZ color space are space coordinates *(X,Y,Z)* analogous to three kinds of the human eyes' *cone cells* which sense light with spectral sensitivity peaks in long (*L*, 560–580 nm), middle (*M*, 530–540 nm) and short (*S*, 420–440 nm) wavelengths[68, 69]. When judging the relative brightness of different colors in well-lit situations, humans eyes tend to perceive green light as brighter than red or blue light of equal power. This is roughly analogous to spectral sensitivity of the *M* cones. In view of this fact, CIE defined *Y* as brightness (luminance) or *M* cone response; *Z* as blue stimulus or *S* cone response and *X* is a mix response of cone response curves [68,69].

The tristimulus XYZ values depend on the observer's field of view. Therefore, the *standard (colorimetric) observer* is defined to represent an average human's chromatic response within a 2° arc inside the *fovea*. This angle was chosen since the color-sensitive cones of the eyes resided within 2° arc of the fovea. Thus, the *CIE 1931 Standard Observer* function is also known as the *CIE 1931 2° Standard Observer*. The chromatic responses of the observer are numerically represented by $\bar{x}(\lambda)$, $\bar{y}(\lambda)$ and $\bar{z}(\lambda)$ called CIE's *color matching functions*. Thus, the tristimulus values for a color with a spectral power distribution *I(λ)* are given as:

$$X = \int_{400}^{700} I(\lambda)\bar{x}(\lambda)d\lambda \quad (1.17)$$

$$Y = \int_{400}^{700} I(\lambda)\bar{y}(\lambda)d\lambda \quad (1.18)$$

$$Z = \int_{400}^{700} I(\lambda)\bar{z}(\lambda)d\lambda \quad (1.19)$$

where λ is the wavelength of the equivalent monochromatic light measured in nanometers [71-74].

Since human eye have three types of cone cells a full plot of all visible colors is a three-dimensional figure. However, the concept of color can be divided into two parts viz. brightness and chromaticity. For example, the color white is a bright color, while the color grey is considered to be a less bright version of that same white color. The chromaticity co-ordinates of a color was then specified by the two derived parameters *x* and *y*, two of the three normalized values which are functions of all three tristimulus values *X*, *Y*, and *Z* [68,69]:

$$x = X/(X+Y+Z) \quad (1.20)$$

$$y = Y/(X+Y+Z) \quad (1.21)$$

$$z = Z/(X+Y+Z) = 1-x-y. \quad (1.22)$$

By calculating the coordinate *(x,y)*, even the color of light corresponding to a complex emission spectrum can be known easily, with the use of the CIE chromaticity diagram.

For a typical determination of CIE space coordinate *(x,y)*, emission data, from 400 to 700 nm, of the sample are used to calculate tristimulus XYZ values. This can be done by using a CIE *coordinate calculator*. Then the coordinate *(x,y)* is calculated by using the above equations. Comparison of the color observed by naked eye and color determined from CIE diagram ensures that the recorded spectra are correct or incorrect. If the two colors are same then the recorded spectrum is correct. However, if the two colors are different the recorded spectrum is incorrect. The comparison is very important since the recorded spectrum may have number of artifacts viz. stray light, second order effect and other instrumental errors which may alter the purity of the spectrum. Hence, CIE chromaticity diagram and coordinate help in recording correct emission spectrum of the sample. Further, the calculated CIE coordinate can be used for determination of *correlated color temperature* (CCT) describe below [68,69,75,76].

1.9 Correlated Color Temperature (CCT)

Color of light emitted from a black body depends on the temperature of the black body [77-80]. Color temperature is the surface temperature of a black body *(Planckian) radiator* which emits the color. It is expressed in *kelvins* (K) or *mired* (milli-reciprocal kelvins). This allows the definition of a standard by which light

sources are compared. By taking analogy with the color temperature of the Planckian radiator, non-Planckian light sources, like fluorescence lamp and LED, are judged by their CCT values. CCT is the color temperature of the non-Planckian light sources which to human color perception most closely resembles the light from the Planckian radiator [68,69,75,76,81-84]. **Table 1.2** list some light sources with its CCT [75,81].

Table 1.2: Light sources and corresponding CCT values.

CCT (K)	**Light Source**
4100–4150	Moonlight
5000	Horizon daylight
5000	Tubular fluorescent lamps or cool white/daylight compact fluorescent lamps (CFL)
5500–6000	Vertical daylight, electronic flash
6200	Xenon short-arc lamp
6500	Daylight, overcast
5500–10500	LCD or CRT screen

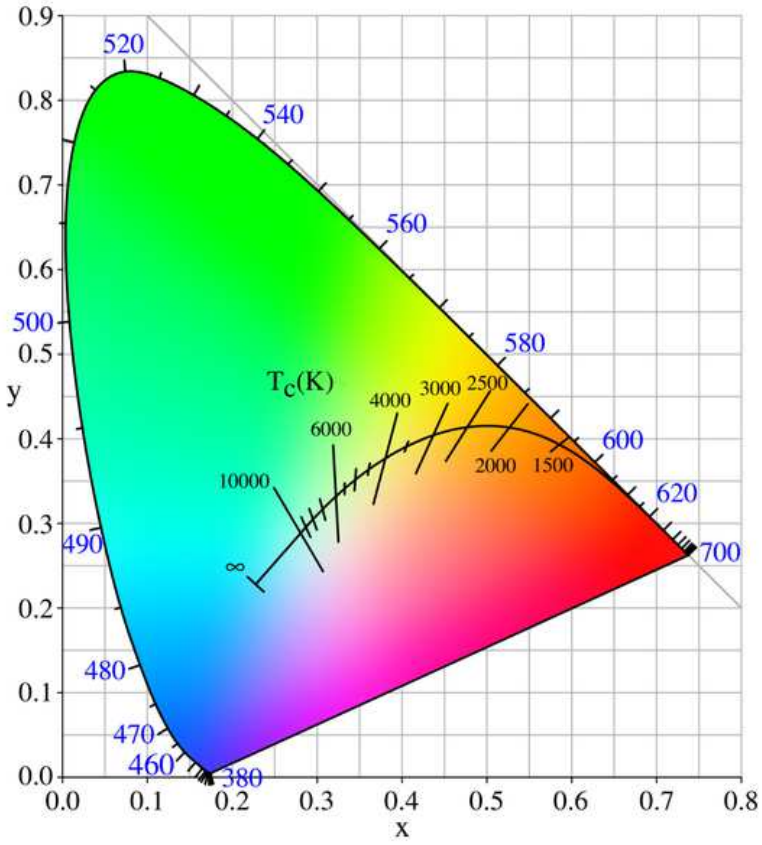

Figure 1.11: CIE diagram showing Planckian locus and isotherms.

The CCT can be calculated for any chromaticity coordinate. However, the result is meaningful only if the light sources are *white* or nearly white. If the light source is white or nearly white, CCT can be approximated from *Planckian locus* of the CIE chromaticity diagram [68,69,75,76,81,85-87]. **Figure 1.11** shows the Planckian locus of the CIE chromaticity diagram. The lines perpendicular to the Planckian locus is called *isotherm lines* and they nearly converge towards a point on the chromaticity diagram. A slope line can be drawn by joining the point and the coordinate *(x,y)* in quest. With this slope, CCT at the coordinate *(x,y)* can be calculated by using the approximation:

$$CCT\ (x,y) = -449n^3 + 3525n^2 - 6823.3n + 5520.33 \quad (1.23)$$

where $n = (x - x_e)/(y - y_e)$ is inverse of the slope line and $(x_e = 0.3320, y_e = 0.1858)$ is the convergent point [78,79,81].

1.10 Scope of the Thesis

In the present work, ZrO_2 and ZrO_2:Eu^{3+} nanocrystals are synthesized by wet chemical techniques viz. simple precipitation, polyol and hydrothermal techniques. The sizes of the nanocrystals are controlled by dopant, Eu^{3+}, concentration and/or annealing temperature. Properties of the nanocrystals are tuned and/or probed as a function of the dopant concentration and/or crystal size. The synthesized nanocrystals are characterized by XRD, TEM, HRTEM, SAED, EDAX on SEM, FTIR, PL spectroscopy, etc. Characterizations of the samples by PL spectroscopy include excitation and emission scans, lifetime, quantum yield, CIE, CCT, etc. Each chapter of the thesis contains introductions and motivations to the basic subject area under study. The chapters are self contain and can be read independently.

References

[1] Illustrated Oxford Dictionary, Rev. Ed. Ed., Dorling Kindersley, London, 2003.

[2] C.P. Poole, F.J. Owens, Introduction to Nanotechnology, John Wiley & Sons, Inc., New Jersey, U.S.A., 2003.

[3] E.L. Wolf, Nanophysics and Nanotechnology: An Introduction to Modern Concepts in Nanoscience, Wiley-VCH, Weinheim, Germany, 2004.

[4] http://www.britishmuseum.org.

[5] http://www.youtube.com/watch?v=4eRCygdW--c.

[6] W.A. Goddard, Handbook of Nanoscience, Engineering, and Technology, CRC, Boca Raton ; London, 2003.

[7] E. Drexler, C. Peterson, G. Pergamit, Unbounding the Future: The Nanotechnology Revolution, William Morrow and Company, Inc., New York, 1991.

[8] A.K. Geim, K.S. Novoselov, Nature Mater., 6 (2007) 183.

[9] H.W. Kroto, J.R. Heath, S.C. O'Brien, R.F. Curl, R.E. Smalley, Nature, 318 (1985) 162.

[10] S. Iijima, Nature, 354 (1991) 56.

[11] K.S. Novoselov, A.K. Geim, S.V. Morozov, D. Jiang, Y. Zhang, S.V. Dubonos, I.V. Grigorieva, A.A. Firsov, Science, 306 (2004) 666.

[12] http://www.nanotec.org.uk/report/Nano%20report%202004%20fin.pdf.

[13] E. Roduner, Chem. Soc. Rev., 35 (2006) 583.

[14] L. Pavesi, L. Dal Negro, C. Mazzoleni, G. Franzo, F. Priolo, Nature, 408 (2000) 440.

[15] S. Tiwari, F. Rana, H. Hanafi, A. Hartstein, E.F. Crabbé, K. Chan, Appl. Phys. Lett., 68 (1996) 1377.

[16] J.W. Stouwdam, Ph.D. Thesis, Faculty of Science and Technology, University of Twente, Enschede, The Netherlands2003.

[17] G. Blasse, B.C. Grabmaier, Luminescent Materials, Springer, Berlin ; London, 1994.

[18] C. Ronda, Luminescence: From Theory to Applications, Wiley-VCH, Weinheim, Germany, 2008.

[19] N.S. Singh, Ph.D. Thesis, Department of Physics, Manipur University, Manipur, India2011.

[20] L.R. Singh, Ph.D. Thesis, Department of Physics, Manipur University, Manipur, India2007.

[21] J.R. Lakowicz, Principles of Fluorescence Spectroscopy, 3rd Ed., Springer, Singapore, 2006.

[22] FLSP920 Series User Guide (Revision 3), Edinbunburgh Instruments Ltd., Livingston, U.K., 2011.

[23] Technical Note 21-1: Guide for Absolute QY Measurements of Liquids, Edinburgh Instruments Ltd., Livingston, U.K.

[24] Operating Instructions, Measurement of Fluorescence Quantum Yield using the Integrating Sphere, Issue 2, Edinburg Instruments Ltd., Livingston, U.K., 2012.

[25] M.H.V. Werts, Sci. Prog., 88 (2005) 101.

[26] K. Smits, L. Grigorjeva, D. Millers, A. Sarakovskis, A. Opalinska, J.D. Fidelus, W. Lojkowski, Opt. Mater., 32 (2010) 827.

[27] K. Kompe, H. Borchert, J. Storz, A. Lobo, S. Adam, T. Moller, M. Haase, Angew. Chem., 42 (2003) 5513.

[28] D.K. Chatterjee, A.J. Rufaihah, Y. Zhang, Biomaterials, 29 (2008) 937.

[29] F. Chen, P. Huang, Y.J. Zhu, J. Wu, C.L. Zhang, D.X. Cui, Biomaterials, 32 (2011) 9031.

[30] N.S. White, R.J. Errington, Adv. Drug Deliver. Rev., 57 (2005) 17.

[31] M. Das, G. Sumana, R. Nagarajan, B.D. Malhotra, Appl. Phys. Lett., 96 (2010) 133703.

[32] R. Gillani, B. Ercan, A. Qiao, T.J. Webster, Int. J. Nanomed., 5 (2010) 1.

[33] Y. Al-Khatatbeh, K.K.M. Lee, B. Kiefer, Phys. Rev. B, 81 (2010) 214102.

[34] E. De la Rosa, L.A. Diaz-Torres, P. Salas, R.A. Rodríguez, Opt. Mater., 27 (2005) 1320.

[35] S. Mandal, M.V. Lee, J.P. Hill, A. Vinu, K. Ariga, J. Nanosci. Nanotechno., 10 (2010) 21.

[36] H.Q. Cao, X.Q. Qiu, B. Luo, Y. Liang, Y.H. Zhang, R.Q. Tan, M.J. Zhao, Q.M. Zhu, Adv. Func. Mater., 14 (2004) 243.

[37] L. Chen, Y. Liu, Y. Li, J. Alloys Compd., 381 (2004) 266.

[38] L. Kumari, W. Li, D. Wang, Nanotechnology, 19 (2008) 195602.

[39] P.F. Manicone, P. Rossi Iommetti, L. Raffaelli, J. Dent., 35 (2007) 819.

[40] A.G. Karaulov, T.M. Shlyakhova, E.I. Akselrod, Refractories, 36 (1995) 29.

[41] I.K. Denry, J. R. Kelly, Dent. Mater., 24 (3) (2008) 299.

[42] K. Jirapattarasilp, J. Rukijkanpanich, Int. J. Adv. Manuf. Technol., 33 (2007) 1136.

[43] D.E. Harrison, N.T. Melamed, E.C. Subbarao, J. Electrochem. Soc., 110 (1963) 23.

[44] X. Chen, L. Li, Y. Su, G. Li, J. Nanosci. Nanotechnol., 10 (2010) 1800.

[45] X. Lu, K. Liang, S. Gu, Y. Zheng, H. Fang, J. Mater. Sci., 32 (1997) 6653.

[46] J. Alarcón, J. Mater.Sci., 36 (2001) 1189.

[47] V.V. Srdic, M. Winterer, Chem. Mater., 15 (2003) 2668.

[48] D. Simeone, G. Baldinozzi, D. Gosset, M. Dutheil, A. Bulou, T. Hansen, Phys. Rev. B, 67 (2003) 064111.

[49] J. Joo, T. Yu, Y.W. Kim, H.M. Park, F. Wu, J.Z. Zhang, T. Hyeon, J. Am. Chem. Soc., 125 (2003) 6553.

[50] M.N. Luwang, R.S. Ningthoujam, S.K. Srivastava, R.K. Vatsa, J. Mater. Chem., 21 (2011) 5326.

[51] Y. Su, L. Li, G. Li, J. Liu, X. Chen, W. Hu, G. Liu, J. Nanosci. Nanotechno., 10 (2010) 1877.

[52] C. Kittel, Introduction to Solid State Physics, 8th Ed., Wiley, Hoboken, NJ, 2005.

[53] P. Scherrer, Göttinger Nachrichten Gesell., 2 (1918) 98.

[54] A.L. Patterson, Phys. Rev., 56 (1939) 978.

[55] K. Byrappa, M. Yoshimura, Handbook of Hydrothermal Technology: A Technology for Crystal Growth and Materials Processing, Noyes Publications, New York, U.S.A., 2001.

[56] Y.R. Devi, Ph.D. Thesis, Department of Physics, Manipur University, Manipur, India2013.

[57] B.D. Cullity, Elements of X-ray Diffraction, Addison-Wesley Pub. Co., Massachusetts, U.S.A., 1956.

[58] R. Erni, M.D. Rossell, C. Kisielowski, U. Dahmen, Phys. Rev. Lett., 102 (2009) 096101.

[59] J.C.H. Spence, Experimental High-resolution Electron Microscopy, Oxford University Press, New York, 1980.

[60] C. Kisielowski, B. Freitag, M. Bischoff, H. van Lin, S. Lazar, G. Knippels, P. Tiemeijer, M. van der Stam, S. von Harrach, M. Stekelenburg, M. Haider, S. Uhlemann, H. Müller, P. Hartel, B. Kabius, D. Miller, I. Petrov, E.A. Olson, T. Donchev, E.A. Kenik, A.R. Lupini, J. Bentley, S.J. Pennycook, I.M. Anderson, A.M. Minor, A.K. Schmid, T. Duden, V. Radmilovic, Q.M. Ramasse, M. Watanabe, R. Erni, E.A. Stach, P. Denes, U. Dahmen, Microsc. Microanal., 14 (2008) 469.

[61] C. Viti, J. Struct.Geol., 33 (2011) 1715.

[62] J. Goldstein, Scanning Electron Microscopy and X-ray Microanalysis, 3rd Ed., Kluwer Academic/Plenum Publishers, New York, 2003.

[63] E.J. Cook, Ph.D. Thesis, University College London, University of London, London, United Kingdom2008.

[64] C.N. Banwell, E.M. McCash, Fundamentals of Molecular Spectroscopy, 4th Ed., McGraw-Hill, London ; New York, 1994.

[65] K. Nakamoto, Infrared and Raman Spectra of Inorganic and Coordination Compounds, 5th Ed., Wiley, New York, 1997.

[66] N.B. Colthup, L.H. Daly, S.E. Wiberley, Introduction to Infrared and Raman Spectroscopy, Academic Press, New York ; London, 1964.

[67] FL WinLab Software User's Guide, PerkinElmer Ltd., Bucks, U.K., 2006.

[68] J. Schanda, Colorimetry: Understanding the CIE System, Wiley ; Chichester : John Wiley, New Jersy, U.S.A., 2007.

[69] R.M. Davis, Choice: Curr. Rev. Acad. Lib., 45 (2008) 1005.

[70] J.C. de Mello, H.F. Wittmann, R.H. Friend, Adv. Mater., 9 (1997) 230.

[71] A.C. Harris, I.L. Weatherall, J. Roy. Soc. New Zeal., 20 (1990) 253.

[72] J. Guild, Philos. T. R. Soc. Lond., 230 (1932) 149-187.

[73] J.G. Holmes, P. Phys. Soc., 47 (1935) 400.

[74] T. Smith, J. Guild, Trans. Opt. Soc., 33 (1931) 73.

[75] P.D. Pinto, J.M. Linhares, S.M. Nascimento, J. Opt. Soc. Am. A, 25 (2008) 623.

[76] P.J. Pardo, E.M. Cordero, M.I. Suero, A.L. Perez, J. Opt. Soc. Am. A, 29 (2012) A209.

[77] T. Kogure, K.-C. Leung, The Astrophysics of Emission-line Stars, Springer, New York, 2007.

[78] K.L. Kelly, J. Opt. Soc. Am., 53 (1963) 999.

[79] C.S. McCamy, Color Res. Appl., 17 (1992) 3.

[80] https://en.wikipedia.org/wiki/Black-body_radiation.

[81] http://en.wikipedia.org/wiki/Color_temperature.

[82] W.R. Stevens, Principles of Lighting, Constable, London, 1951.

[83] E.P. Hyde, Phys. Rev., 32 (1) (1911) 632.

[84] I.G. Priest, J. Opt. Soc. Am., 7 (1923) 1175.

[85] W. Walter, Color Res. Appl., 17 (1992) 24.

[86] H. Akamine, J. Morishita, M. Matsuyama, Y. Nakamura, N. Hashimoto, F. Toyofuku, Med. Phys., 39 (2012) 5127.

[87] B. Wu, X. Luo, H. Zheng, S. Liu, Opt. Express, 19 (2011) 24115.